Science of the Total Environment 729 (2020) 138635

Contents lists available at ScienceDirect

Science of the Total Environment

journal homepage: www.elsevier.com/locate/scitotenv

Estimating daily evapotranspiration in the agricultural-pastoral ecotone in Northwest China: A comparative analysis of the Complementary Relationship, WRF-CLM4.0, and WRF-Noah methods

Xuefeng Xu [a], Xuliang Li [a], Xuejin Wang [a], Chansheng He [a,b,*], Wei Tian [a], Jie Tian [a], Lixiao Yang [a]

[a] Key Laboratory of West China's Environmental System (Ministry of Education), College of Earth and Environmental Sciences, Lanzhou University, Lanzhou, Gansu 730000, China
[b] Department of Geography, Western Michigan University, Kalamazoo, MI 49008, USA

HIGHLIGHTS

- Estimating actual ET in APENC with heterogeneous surface is difficult but essential.
- Three methods with different complexity were compared and assessed.
- The WRF-CLM4.0 and CR model show a better applicability than WRF-Noah in the APENC.
- The CR model is well-suited for data lacking, heterogeneous landscapes such as the APENC.

GRAPHICAL ABSTRACT

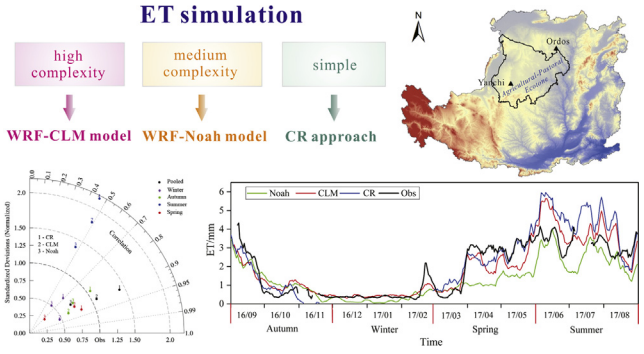

ARTICLE INFO

Article history:
Received 11 November 2019
Received in revised form 8 April 2020
Accepted 9 April 2020
Available online 28 April 2020

Editor: Paulo Pereira

Keywords:
Daily regional ET
Complementary relationship
Community land model
Noah model
Weather research and forecasting
Agricultural-pastoral ecotone in Northwest China

ABSTRACT

Accurate estimation of evapotranspiration (ET) over regional scale is essential for ecohydrological research, agricultural production, and water resources management. However, few studies have been done to estimate regional ET in data lacking, highly heterogeneous arid areas such as the Agricultural-Pastoral Ecotone in Northwest China (APENC). In this study, we compared three actual ET-estimation methods driven by Weather Research and Forecasting (WRF) model in a semi-arid region. We selected the state of the art Weather Research and Forecasting-Community Land Model 4.0 (WRF-CLM4.0) model, the widely used WRF-Noah model and an empirical Complementary Relationship (CR) model to compare their model structures and mechanisms of estimating daily ET in the study region. The WRF model was chosen to address the problem of data scarcity in the study region and to derive model input for ET estimation with high spatial resolution. The seasonal and pooled performances of the three models were verified with in situ observations. Results indicate that the WRF-CLM4.0 model shows a better applicability in the study region, with a superior performance for the pooled datasets (Pearson correlation coefficient [r] = 0.89, root-mean-square error [RMSE] = 0.66 mm/d and Nash-Sutcliffe efficiency coefficient [NSE] = 0.90), while the CR model has a comparable performance (r = 0.91, RMSE = 0.86 mm/d and NSE = 0.85) and the WRF-Noah model shows the worst performance (r = 0.82, RMSE = 0.94 mm/d and NSE = 0.81). The differences are mainly caused by different representations of the land surface characteristics and hydrology of the study region by the three different models. Our analysis shows that the WRF-CLM4.0 model and the CR model are more applicable to the APENC than the WRF-Noah model. For regional

* Corresponding author at: Key Laboratory of West China's Environmental System (Ministry of Education), College of Earth and Environmental Sciences, Lanzhou University, Lanzhou, Gansu 730000, China.
E-mail address: he@wmich.edu (C. He).

https://doi.org/10.1016/j.scitotenv.2020.138635

applications, the CR model, with fewer parameters and simpler structure, is able to capture the local characteristic and well-suited for data lacking, highly heterogeneous landscapes such as the APENC.

1. Introduction

Evapotranspiration (ET) is an essential variable for understanding the variation of the atmosphere (weather and climate), the land surface processes (water and energy balance) and interactions between the land surface and atmosphere (Wang and Dickinson, 2012; Fisher et al., 2017). It affects atmospheric dynamics, impacts hydrologic processes and water cycles, and alters magnitude and distribution of agricultural and ecosystem productivity and services over different spatial and temporal scales (Thakur et al., 2012; Allen et al., 2011; Fisher et al., 2017). The global and regional climate and environmental changes have altered terrestrial water balance and energy budget (IPCC, 2014), resulting in increased frequency and magnitude of extreme weather events such as droughts, expanding land degradation and desertification, reducing agricultural productivity and ecosystem services, threatening the global food and water security, particularly in arid and semi-arid regions that account for over 40% of the global land and supports over 2.5 billion people (Reynolds et al., 2007; Kioutsioukis et al., 2016; Fisher et al., 2017). Agricultural-pastoral ecotones (transition areas between farmland grassland) are widely distributed in the arid and semi-arid regions of the world and are especially vulnerable to the impacts of climate and environmental changes. As one of the four largest in the world, the Agricultural-Pastoral Ecotone in Northwest China (APENC) faces a chronical water scarcity (Yang et al., 2016b; Li et al., 2018a, 2018b), making it a fragile ecosystem with grassland degradation and land desertification (Liu et al., 2010; Zhao et al., 2017). ET is a significant factor for understanding the response of terrestrial biosphere to the changes of hydrological and climatological regimes (Fisher et al., 2017). Accurate estimation of regional ET is crucial for developing effective adaptation strategies for better management of agricultural production and protection of grassland ecosystem (Allen et al., 2011; Fu et al., 2011;Thakur et al., 2012; Fisher et al., 2017).

The APENC is one of the largest ecotones in the world (Cao et al., 2015). With highly-heterogeneous land surface and human disturbance (Wang et al., 2020), it has high spatial and temporal variability of ET. Furthermore, owing to a harsh environment and lack of high-density, long-term observational data, only a sparse measurement exists, making accurate simulation of regional ET challenging. Therefore, it is urgent to investigate different methods that can accurately estimate regional ET with relatively high spatial and temporal resolution in the study region.

Over the past few decades, several approaches have been developed to estimate ET at regional scale. First, conventionally, ET can be observed by in suit measurements (e.g., lysimeters and eddy covariance techniques) (Wang and Dickinson, 2012). However, such measurements could be inappropriate for large areas that require plenty of measurement stations. Because of instrumentation and labor cost and resource constraints, in situ observations are often extremely sparse and unevenly distributed in many regions and countries, leading to low spatial resolution ET estimates over larger spatial scales (Simolo et al., 2010), where large variations in land surface processes due to increased landscape heterogeneity cannot be accurately monitored (Srivastava et al., 2016). Second, estimating ET by remote sensing has expanded the knowledge of ET distribution over multiple spatial scales especially at regional scale, but most remote sensing approaches just capture instantaneous ET rates, and upscaling of these instantaneous values to longer time periods runs into uncertainty (Ma et al., 2014, 2015). Third, values of ET can be also estimated by empirical models. Such models include Penman-Monteith equation (Monteith, 1963), Complementary Relationship (CR) methods (Bouchet, 1963) and related models such as the Advection-Aridity (AA) model (Brutsaert and Stricker, 1979). Of the empirical models, the CR approach been applied to different types of land use from grassland (Kahler and Brutsaert, 2006), to cropland (Ozdogan and Salvucci, 2004) and shrublands (Jaksa et al., 2013), and shows a better performance in semi-arid areas (Ma et al., 2015). It requires only a set of meteorological variables, bypassing vegetation and soil parameters and is suitable for estimating ET over large scales (Jaksa et al., 2013). Mesoscale models (Ozdogan et al., 2006) and remote sensing data (Liu et al., 2010) can be used to drive the CR and mitigate the paucity of observation data in sparsely monitored regions (Pan et al., 2012). Xu and Singh (2005) evaluated the performance of the CR method and found that locally calibrated parameter values improved the CR model in the research regions significantly.

Recent development of energy balance-based numerical land surface models (LSMs), which take into account physical and biogeochemical interactions, has expanded the knowledge of estimating ET values at variable spatial-temporal scales and with different degrees of accuracy (Liang et al., 1994; Fisher et al., 2017). LSMs, such as Noah and Community Land Model (CLM), include many plant physiological and biometeorology processes with complex mechanisms and numerical calculations, provide a way to address lacking of reliable input and parameters (e.g., turbulent transfer coefficients and stomatal conductance) that are hard to acquire appropriately at different spatial and temporal scales. Research shows that CLM and Noah model have a better performance in estimating regional ET in semi-arid areas compared to some other LSMs (Yang et al., 2016a; Xiao et al., 2017). Although, LSMs were widely used in land surface process simulation, there are few researches focusing on the simulation, assessment and comparison of ET values at regional scales (Falk et al., 2014). Furthermore, complexity in model structure does not often translate into higher accuracy on model performance due to the increasing uncertainty introduced by a great number of input variables needed by process-based models (Xu et al., 2017; Perrin et al., 2001). Understanding the accuracy of ET estimates in semi-arid areas with models of varying degrees of complexity is essential to select the appropriate ET model(s) to meet the objectives of different studies.

However, in many semi-arid areas, weather station networks with accurate weather data are still in short supply (Simolo et al., 2010; Cruz-Blanco et al., 2015), thus requiring the development of new methodologies at a lower cost than the traditional methods. The Weather Research and Forecasting (WRF) model is a state-of-the-art, mesoscale numerical weather prediction and atmospheric research model (Chen and Dudhia, 2001), which can use reanalysis data to provide meteorological forcing data (Pan et al., 2012), easing the conflict of interpolating limited meteorological observations in sparely monitored regions at large spatial scales. In addition, running in a coupled fashion with some LSMs, the WRF model can be used to simulate land surface process directly. Weather Research and Forecasting-Community Land Model (WRF-CLM) couples the WRF and CLM and considers the feedback of regional ET on atmospheric interactions, enhancing the systematic understanding of land surface process (Falk et al., 2014; Xu et al., 2017). Wu et al., 2018 and Branch et al. (2014) investigated regional surface fluxes (including ET) with WRF-Noah model in both grassland and cropland in semi-arid areas, respectively. The WRF-CLM model can also simulate surface ET over large regions, such as California (Subin et al., 2011) and the Great Plains region (Van Den Broeke et al., 2018), in which WRF-CLM3.5 and WRF-CLM4.0 were used, respectively.

In the APENC, works have explored dynamic land cover changes (ecosystem degradation and reforestation) (Wu et al., 2013; Huang et al., 2013), physiological characteristics of vegetation (Chen et al.,

2016; Liang and Yang, 2016), surface energy budgets (Zhao et al., 2017; Wei et al., 2018) and land surface-atmosphere interactions (Wang et al., 2020). Studies have focused mainly on the estimation of ET under different vegetation types (Li and Li, 2000; Gong et al., 2017) and weather conditions (Yang et al., 2016b) with in situ observations or models at point scale. Few studies estimated ET at regional scale, especially over daily intervals (Liu et al., 2010). To this end, this study uses three models with different complexity: high-complexity WRF-CLM4.0 model, medium-complexity WRF-Noah model and simple empirical CR model to estimate ET rates at regional scale in the APENC. The objectives of the study are: 1) to evaluate the WRF simulated meteorological variables (humidity and air temperature) against the ground-based in situ observations at regional scale; 2) to calibrate the parameters of CR for estimating ET values at regional scale; and 3) to compare the ET results computed by the three models and assess their performances and applicability to the study region.

2. Study area and data

The study region is located in a semi-arid region in Northwest China, ranging from 106.228°E to 110.903°E and 36.816°N to 40.194°N (Fig. 1). And it is also situated in the west of the Loess Plateau. This region has a typical continental semi-arid climate featured by less and instable precipitation (mean annual precipitation of 250–450 mm), high frequency of drought, and sandstorms. Its annual average temperature ranges from 7.0 °C to 9.0 °C (Qi et al., 2012; Wang et al., 2020).

In the study region, semi-arid agriculture and grassland are the dominant land use types, of which corn and Artemisia Ordosica are the main crop and grass species, respectively, and other land cover types include shrubland and desert (Qi et al., 2012). As an agricultural-pastoral ecotone in semi-arid area, the vegetative cover type is very sensitive to anthropogenic influences and changes of climate (Wei et al., 2018). In recent years, ecological protection programs such as “Grain for Green” have been implemented in since 1998 to alleviate land degradation in the study region. Dynamic conversion and mosaic distribution of grassland and farmland produce a highly heterogeneous landscape in the study region. The large variations in land surface processes in the highly heterogeneous landscape, together with lack of in situ observations, make it a challenge to accurately monitor ET directly at regional scale (Li et al., 2018b; Detto et al., 2006).

In this study, we established two in situ observation stations in 2016, Yanchi and Ordos Observation Station, in the study area (Fig. 1). The in situ observations include meteorological and ET measurements. The meteorological data are collected by automatic meteorological station, including precipitation, temperature at 2 m and relative humidity, and the ET values are measured by two lysimeters in different land use types (farmland and grassland). During the research period of 1 August 2016 through 31 August 2017, the Yanchi and Ordos stations had a total precipitation of 430 mm and 270 mm, respectively.

3. Methods

3.1. The Weather Research and Forecasting (WRF) model

As a state-of-the art mesoscale numerical weather modeling system, WRF model was developed by the National Center for Atmospheric Research (NCAR), the National Oceanic and Atmospheric Administration (NOAA), and the Earth System Research Laboratory (ESRL). It can be used for both meteorological research and operational forecasting and hydrological applications (Jin et al., 2010). Higher spatial resolutions (10 km) make WRF more applicable for regional scale weather and climate applications than the global climate models (Wang et al., 2020). For the uses of estimating ET values, WRF could drive empirical ET models (Wu et al., 2016), because it can use reanalysis data to provide meteorological forcing data (Pan et al., 2012), easing the conflict of interpolating limited meteorological observations at sparely monitored regions (especially the APENC) for large spatial scales. Another alternative is to run in a coupled fashion with LSMs, such as WRF-CLM and WRF-Noah.

In this study, simple empirical CR model is driven by meteorological forcing data provided by WRF. Since local calibration of the CR model has not been done at the APENC (Liu et al., 2010), this study first adjusted the parameters in the CR model with measured data. Additionally, preliminary evaluation would be done to test the applicability of the WRF to drive the CR model. And both high-complexity WRF-CLM4.0 model and medium-complexity WRF-Noah model are run in a coupled fashion.

For the model spin-up and analysis, the WRF runs were from 1 August 2016 through 31 August 2017, while the first month was eliminated for model initialization and the rest was divided into four seasons: Autumn (September 2016 to November 2016), Winter

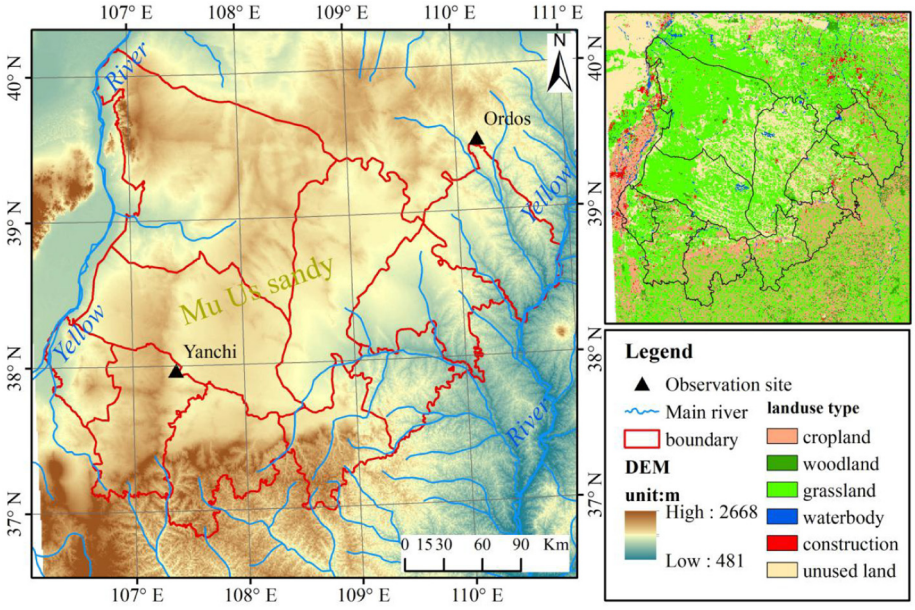

Fig. 1. Map of the study area (boundary and land use types) and two in situ observation stations.

(December 2016 to February 2017), Spring (March 2017 to May 2017), and Summer (June 2017 to August 2017). The WRF model (version 3.8.1) was run at a resolution of 10 km with a two-way nesting scheme. The temporal resolution of output data is 6-hour intervals and was aggregated to daily values. The WRF runs were forced by FiNaL Analysis (FNL) dataset with the same atmospheric forcing except for the land surface schemes.

3.2. WRF-CLM4.0

The coupled WRF-CLM4.0 was developed by the National Center for Atmospheric Research, USA (Oleson et al., 2010; Skamarock et al., 2008). Compared with relatively simple land surface schemes in WRF, newly coupled WRF-CLM model improved the surface process simulation in different spatial scales (Subin et al., 2011; Lu and Kueppers, 2012). It contains sophisticated simulation of biogeophysics, hydrology, biogeochemistry, and vegetation dynamics and is particularly suitable for global and regional applications. In the CLM4.0 scheme, a single-layer vegetation canopy is equipped with 4 plant functional types (PFTs), where each of them has different physiology and structures, and a five-layer snowpack exists. For simulation of ET, the model considers non-vegetated surface and vegetated surface (Xiao et al., 2017) (Table 1). For non-vegetated surface:

$$E_{soil} = -\frac{\beta_{soil}\rho_{atm}(q_{atm}-q_{soil})}{r_{aw}} \tag{1}$$

Where ρ_{atm} is the density of atmospheric air (kg m^{-3}), β_{soil} is a function of the soil moisture; q_{atm} is the atmospheric specific humidity, q_{soil} is the specific humidity of the soil, and r_{aw} is the aerodynamic resistance to water vapor transfer (Sakaguchi and Zeng, 2009).

$$q_{soil} = \alpha_{soil} q_{sat}^{T_1} \tag{2}$$

Where $q_{sat}^{T_1}$ is the saturated specific humidity at the soil surface temperature T_1. And α_{soil} is a function of ψ (Philip, 1957):

$$\alpha_{soil} = exp\left(\frac{\psi_1}{1\times 10^3 R_{wv} T_1}\right) \tag{3}$$

In which R_{wv} is the gas constant of water vapor, $\psi_1$is the soil moisture matric potential. The ψ_1 is:

$$\psi_1 = \psi_{sat,1} s_1^{-B_1} \geq -1\times 10^8 \tag{4}$$

In which $\psi_{sat,\ 1}$ is the saturated matric potential, B_1 is a parameter (Clapp and Hornberger, 1978). The surface wetness of the top soil layer s_1 is:

$$s_1 = \frac{1}{\Delta z_1 \theta_{sat,1}}\left[\frac{w_{liq,1}}{\rho_{liq}} + \frac{w_{ice,1}}{\rho_{ice}}\right] \quad 0.01 \leq s_1 \leq 1.0 \tag{5}$$

In which Δz_1 and are the thickness and the saturated volumetric water content of the top soil layer, respectively, ρ_{liq}, ρ_{ice} and $w_{liq,1}$, $w_{ice,1}$ are the density and mass of liquid water and ice, respectively.

$$\beta = \frac{a - b^{-B_1}}{a-1} \tag{6}$$

$$a = \frac{10^3 R_{wv} T_g \left(\frac{q_{atm}}{q_{sat}^{T_1}} - 1\right)}{\psi_{sat,1} g} \tag{7}$$

$$b = \frac{w_{liq}}{\Delta z_1 \theta_{sat,1} \rho_{liq}} \tag{8}$$

Where β, which is a simplified specific value of actual ET and max ET (without restrict of soil moisture) (Xiao et al., 2017); T_g is the ground temperatures.

The Eqs. (6)–(8) manifest that in the CLM4.0 scheme the parameter β is related to multi-factors other than soil moisture, such as surface temperature, humidity and others.

For vegetated surface:

$$E = -\rho_{atm}\frac{(q_{atm} - q_s)}{r_{aw}} \tag{9}$$

$$q_s = \frac{c_a^w q_{atm} + c_g^w q_g + c_v^w q_{sat}^{T_v}}{c_a^w + c_g^w + c_v^w} \tag{10}$$

Where q_s is canopy specific humidity, c_a^w, c_g^w, c_v^w are the sensible heat conductance from the canopy layer to the atmosphere, the ground to canopy layer, and leaf surface to canopy layer, respectively.

$$\beta = \frac{a - b^{-B_1}}{a-1} \tag{11}$$

$$a = \frac{10^3 R_{wv} T_g}{\psi_{sat,1} g}\left(\frac{\left(c_v^w + c_g^w\right) q_{atm} - c_v^w q_{sat}^{T_v}}{c_g^w q_{sat}^{T_g}} - 1\right) \tag{12}$$

$$b = \frac{w_{liq}}{\Delta z_1 \theta_{sat,1} \rho_{liq}} \tag{13}$$

This is similar to bare soil evaporation, while some difference exists in the calculation of parameter a.

The effect of snow to ET is also important. The CLM model has a sophisticated snow compaction scheme and physical description of frozen soil processes. The energy balance equation in the model to compute the snowmelt is as follow (Oleson et al., 2004):

$$(1-\alpha_s)S_0\downarrow + (LWD_{a+v} - LWU) - H - LE - G - H_m = 0 \tag{14}$$

Where α_s is the surface albedo of snow and soil; $S_0\downarrow$ is fractional downward solar radiation to the surface; $LWD_{a+\ v}$ and LWU are the downward long-wave radiation and emission from the surface,

Table 1
Comparison of the ET calculating in CLM, Noah, and CR model.

Model	Complexity	Mode of soil moisture	Snow-melt module
CLM	High complexity (including non-vegetated surface evaporation, vegetation ET and ground evaporation of vegetated surface)	A power function	5-layer snow with liquid water; variable snow density
Noah	Medium complexity (including bare soil evaporation and canopy ET)	A linear form	1-layer snow lumped with the topsoil layer; fixed snow density
CR	Simple (calculating ET directly)	None	None

respectively; H, LE and G are the sensible heat flux, latent heat flux and ground heat flux, respectively; H_m is the heat flux for the snowmelt (Oleson et al., 2004).

3.3. WRF-NOAH

The Noah Scheme is one of the "second generation" land surface models of the WRF which represents the main processes of plant and soil on ET, soil moisture and snow in the land surface. It has one canopy layer and four soil layers to capture the moisture and temperature at the canopy and soil layers for surface energy closures and water budgets. The Noah scheme which is incorporated in WRF makes use of the Penman equation to simulate ET (Chen and Dudhia, 2001) (Table 1).

The direct evaporation from the ground surface is:

$$E_{dir} = (1-\sigma_f)\beta E_p \tag{15}$$

$$\beta = \frac{\theta_1 - \theta_w}{\theta_{ref} - \theta_w} \tag{16}$$

In which E_p is estimated with method of Penman called a potential evaporation; θ_{ref} is the field capacity point, θ_w is wilting point; σ_f is the green vegetation fraction.

The canopy ET is determined by:

$$E_t = \sigma_f E_p B_c \left[1-\left(\frac{W_c}{S}\right)^n\right] \tag{17}$$

Where W_c is the intercepted canopy water content and B_c is calculated as:

$$B_c = \frac{1+\frac{\Delta}{R_r}}{1+R_c C_h + \frac{\Delta}{r}} \tag{18}$$

Where C_h is the exchange coefficient between water and energy; R_r is defined by a formula of the air temperature, surface pressure and C_h; Δ is the slope of the saturation vapor pressure curve at air temperature; and R_c is the canopy resistance, calculated here following Eq. (20):

$$R_c = \frac{R_{c\ min}}{LAI F_1 F_2 F_3 F_4} \tag{19}$$

Where F_1, F_2, F_3 and F_4 express the effects of solar radiation, vapor pressure deficit, air temperature and soil moisture, ranging from 0 to 1 (Jacquemin and Noilhan, 1990).

$$\beta = \frac{F_4(a+1)}{F_4 a + 1} \tag{20}$$

$$a = \frac{\frac{\Delta}{R_r C_n}(LAI F_1 F_2 F_3)}{R_{c\ min}} \tag{21}$$

For both bare surface and canopy, Eqs. (17), (20)–(22) show that soil moisture affects ET in a linear manner.

In Noah model, the snow scheme has just one layer of snow cover. On snow-atmosphere and snow-soil interfaces, it simulates the accumulation, sublimation and melting of snow, and heat exchange at the same time. The snowmelt is computed below:

$$(1-\alpha_g)S_g\downarrow + (LWD_a - LWU) - H - L - H_m = 0 \tag{22}$$

Where α_g is the albedo of the land surface; $S_g\downarrow$ and LWD_a are the downward solar radiation and the downward longwave radiation (Smirnova et al., 1996; Chen and Dudhia, 2001).

3.4. CR approach

Bouchet (1963) proposed the complementary relationship of ET. The feedback between actual evapotranspiration and potential evapotranspiration (ET_p) can be expressed by: $2ET_w = ET_p + ET_a$., where ET_w is the wet environment ET (Table 1).

Since then, it has been widely applied under different climate and surface conditions because it doesn't need considering complex interactions of surface-atmosphere and avoids calculation of hard to measure vegetation parameters such as canopy resistance parameter (Ma et al., 2015).

For the formula of $2ET_w = ET_p + ET_a$, the ET_p is an equation by the Penman (1948) which is:

$$ET_p = \frac{\Delta(R_n - G)}{(\Delta+\gamma)} + \frac{\gamma f(U)(e_0 - e_a)}{(\Delta+\gamma)} \tag{23}$$

Where Δ and γ are the slope of the vapor pressure curve and the psychrometric constant, respectively. R_n and G are net radiation and soil heat flux. e_o and e_a are the saturation and actual vapor pressure of the air. $f(U)$ is formulated as (Brustaert, 1982)

$$f(U) = 2.6(1 + 0.54U_2) \tag{24}$$

ET_w is wet environment ET using Priestley-Taylor formula (Priestley and Taylor, 1972)

$$ET_w = \frac{\alpha(R_n - G)}{(\Delta+\gamma)} \tag{25}$$

Where ET_w is ET at the wet environment, α is defined by Priestley and Taylor (1972), with a default value of 1.26 generally. In this study, parameter α was estimated with the observed ET values following (Ma et al., 2015), that on wet days, when ET is close to ETp and therefore to ET_w, it can be estimated from the observed ET values, thus $\alpha = 1.23$ in this study.

For a dimensionless expression which is needed for an accurate universal relationship (Kahler and Brutsaert, 2006), the CR was normalized by scaling the ET_p and ET by the ET_w: $E_{MI} = ET / ET_p$; $E_+ = ET / ET_w$; $ET_{p+} = ET_p / ET_w$.

Table 1 summarizes the main differences between the WRF-CLM, WRF-Noah, and CR in model structure, soil moisture and snow-melt modules.

3.5. Budyko approach

The Budyko approach shows the partitioning of the mean annual precipitation to ET (Budyko, 1974). The general expression of the Budyko approach takes into account the characteristics of the basin and uses the surface parameter (α) to characterize different basins (Gao et al., 2016). The form developed by Fu, 1981 is widely used and the equation is:

$$\frac{ET}{P} = 1 + \frac{ET_p}{P} - \left[1 + \left(\frac{ET_p}{P}\right)^{\alpha}\right]^{1/\alpha} \tag{26}$$

Where P is the precipitation, ET_p/P is the aridity index. And the parameter α is the landscape characteristics.

3.6. Model evaluation approach

Since daily meteorological variables are needed to implement the CR model, we ran the WRF model over the research region, and aggregated the hourly WRF downscaled weather variables to daily scale. Subsequently, two weather variables required by the CR model (temperature at 2 m and relative humidity) were validated with in situ measurements

in the Ordos Observation Station. Pearson correlation coefficient (r), root-mean-square error (RMSE) and mean bias error (MBE) were chosen as evaluation indices.

$$r = \frac{\sum_{i=1}^{n}\left(X_i^{obs}-\overline{X}_i^{obs}\right)\left(X_i^{sim}-\overline{X}_i^{sim}\right)}{\sqrt{\sum_{i=1}^{n}\left(X_i^{obs}-\overline{X}_i^{obs}\right)^2}\sqrt{\sum_{i=1}^{n}\left(X_i^{sim}-\overline{X}_i^{sim}\right)^2}} \quad (27)$$

$$RMSE = \sqrt{\frac{1}{n}\sum_{i=1}^{n}\left(X_i^{obs}-X_i^{sim}\right)^2} \quad (28)$$

$$MBE = \frac{1}{n}\sum_{i=1}^{n}\left(X_i^{obs}-X_i^{sim}\right) \quad (29)$$

Where X_i^{obs} and $\overline{X}_i^{obs}$ are observed values and the average observed data during the research period, respectively. X_i^{sim} and $\overline{X}_i^{sim}$ are simulated values and the average simulated data during the research period, respectively.

To evaluate performance of ET modeling, r and RMSE were chosen as seasonal evaluation indices, and r, RMSE and Nash-Sutcliffe efficiency coefficient (NSE) were chosen for pooled evaluation. The Taylor diagram (Taylor, 2001) is used to show the comparison of the simulated ET by the WRF-CLM4.0, WRF-Noah and the CR to the in situ observations. It includes indices r and normalized standard deviation (NSD). The arcs in the diagrams show correlation coefficients, while the horizontal and vertical axes indicate the ratio of the standard deviation (SD) of the simulated data to the observations (Wang et al., 2020). The model performs better when the NSD is close to one, representing the same standard deviation value as that of the observations. In this study, two software were used to calculate the evaluation indices that are the NCAR Command Language (NCL) and Excel.

$$NSE = 1-\frac{\sum_{i=1}^{n}\left(X_i^{obs}-X_i^{sim}\right)^2}{\sum_{i=1}^{n}\left(X_i^{obs}-\overline{X}_i^{obs}\right)^2} \quad (30)$$

$$SD = \sqrt{\frac{1}{n}\sum_{i=1}^{n}\left(X_i-\overline{X}\right)^2} \quad (31)$$

$$NSD = \frac{SD_{sim}}{SD_{obs}} \quad (32)$$

Where SD_{sim} and SD_{obs} are the simulated and observed values of standard deviation, respectively.

4. Results and discussion

4.1. Evaluation of applicability of WRF model in the study area

Evaluation of the applicability of the WRF model in the study region is shown in Fig. 2 for validation of the WRF downscaled daily air temperature and relative humidity (RH) in the study area. The simulated air temperature shows a good agreement with the observation in the scatter diagram and the values of r, MBE, and RMSE are 0.93 (significant at $\alpha = 0.05$), 1.77 °C and 1.07 °C, respectively. It is worth noting that there is an overall overestimation only when air temperature was low, although the deviation is relatively small. Fig. 2c shows variations of the differences of the simulated and observed air temperature with time. As seen in Fig. 2c, the simulated air temperature well matched the observed air temperature in summer when the air temperature

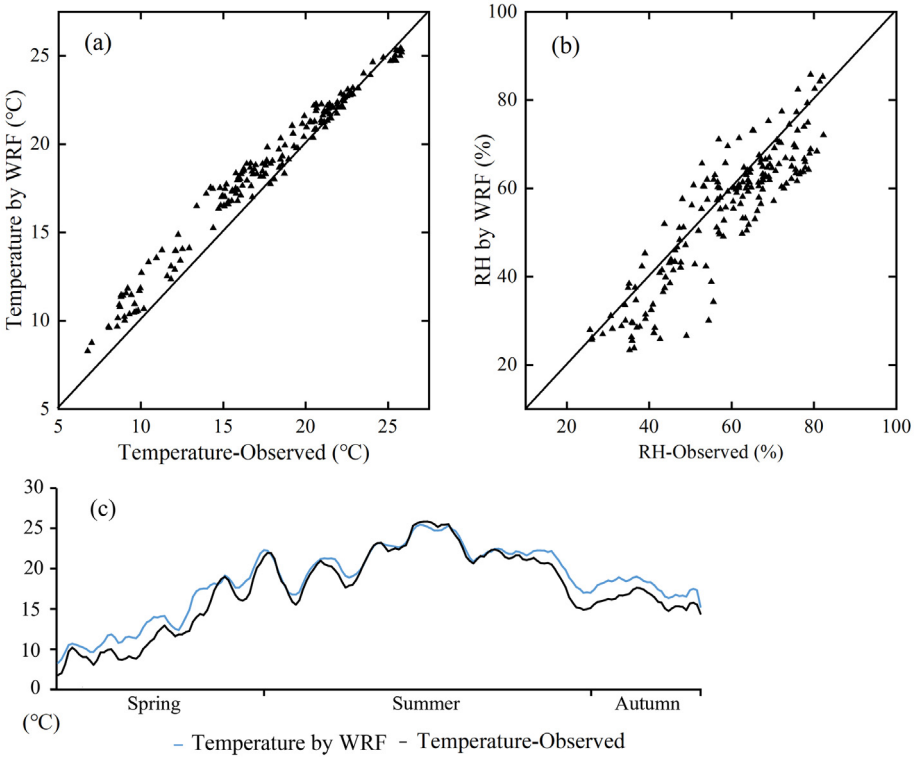

Fig. 2. Comparisons of the simulated air temperature by WRF and observed air temperature at Ordos station from March to September of 2017 (a), the simulated RH by WRF and observed RH for the same period (b), and comparison of the time series of the simulated air temperature and observed air temperature for the same period (blue line represents the simulated air temperature, and black line represents the observed air temperature). (For interpretation of the references to color in this figure legend, the reader is referred to the web version of this article.)

was high but showed overestimation in spring and autumn when the values of air temperature were relatively low, which is similar to the results published previously (Lu and Kueppers, 2012; Van Den Broeke et al., 2018). The values of r, MBE and RMSE between the downscaled RH and in situ observations at the Ordos Observation Station are 0.81 (significant at $\alpha = 0.05$), 9.6% and 3.03%, respectively. And there is no overall overestimation or underestimation. The results demonstrate that the downscaled simulation is reasonable and can be used in the CR model.

4.2. Local calibration and preliminary evaluation of the CR model

The local influence of the key parameter values in the CR model is important to obtaining the actual complementary relationship in the semiarid regions (Ma et al., 2015). Thus, it is necessary to specify α for local conditions in the study area. Meteorological data from the Ordos Observation Station were first aggregated to the daily time steps and then used to compute ET_p and ET_w, respectively. And parameter α was estimated with the observed ET values following (Ma et al., 2015), $\alpha = 1.23$. Potential complementary feedbacks were sought with analyzing the actual relationship of observed ET and ET_p as a function of the E_{MI} at Ordos Observation Station. Daily ET_p and ET versus E_{MI} spanning from 1 September 2016 to 1 September 2017 at Ordos Observation Station are plotted in Fig. 3a.

To make the formulation dimensionless (Kahler and Brutsaert, 2006), scaled ET_p and ET is shown in Fig. 3b, where a complementary relationship between ET_p and ET clearly exists. However, a number of scatter and asymmetric behaviors still exist. The scatter happens in winter months in which the ET_w is low and ET_p is relatively high, which inflates the ET_p/ET_w ratio, making the CR invalid during these periods. Huntington et al. (2011) states that the dynamic equilibrium between the near surface boundary and the land surface could be decoupled by weather fronts. Jaksa et al. (2013) excludes winter month from the analysis because of passing weather systems and potential decoupling between the land surface and the atmosphere. Because the presence of winter data in the E_+ resulted in extremely low ET_w values and large ET_p values, possibly from dry windy conditions, and greatly increased the ET_p/ET_w ratio, data of winter periods (December–February) were eliminated in our study. Fig. 3c shows a better consistency CR between ET and ET_p after eliminating values of the winter months. Normalized E_+ and ET_{p+} in Fig. 3d illustrate a complementary behavior with less scatter in the plot after data from winter periods were eliminated.

Fig. 4 illustrates 1:1 plot of observed and simulated daily ET using the data of March 2017 to September 2017. The modeled ET rates are relatively larger than the measured daily ET values when ET values are high, and smaller when ET values are low, although their agreement is good with r of 0.81 (significant at $\alpha = 0.05$), RMSE of 0.39 mm/d and NSE of 0.90. However, the bias may be from accumulations of errors from the simulated input data.

To address the bias in the CR-simulated ET values, we followed the work of Ma and Szilagyi (2019) to analyze how possible biases in the forcing data (temperature at 2 m and relative humidity) impact the modeling results. At the sensitivity analysis, the CR method was rerun with altering one input parameter while retaining other parameters unperturbed. The results show that the CR model is more sensitive to air temperature, as a 10% increase in air temperature would cause ET values to vary by −6.33% on average. And for relative humidity, a 10% increase only leads to 4.56% change in the ET values. This analysis partly explains the bias of the CR-simulated ET values driven by the WRF model. During the period when air temperature is low, the ET values usually are low in

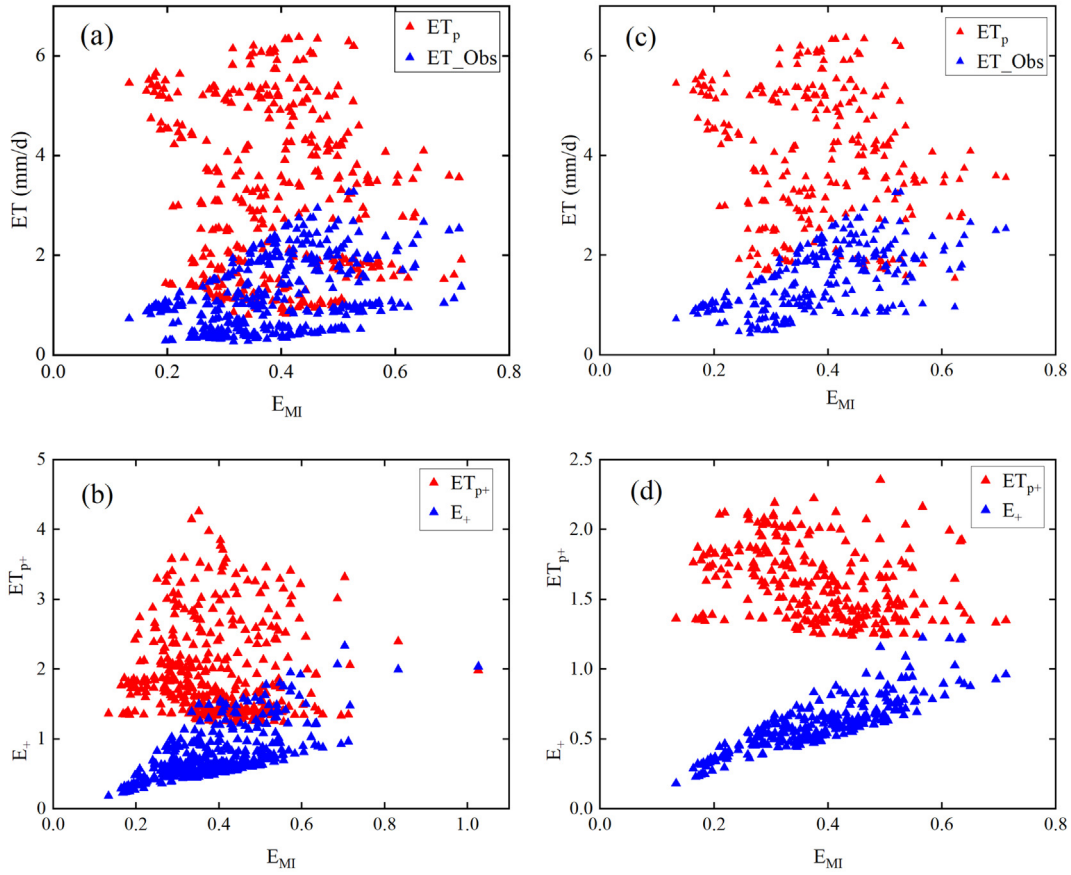

Fig. 3. The nonormalized and normalized CR against the humidity index *Ei* at Ordos Station. (a) Observed daily ET and estimated potential ET rates. (b) Normalized daily actual *E*+ and estimated potential *ETp*+ rates. (c) Observed daily ET and estimated *ETp* excluding winter months (December–February). (d) Normalized daily actual *E*+ and estimated potential *ETp*+ rates, excluding data from winter months (December–February).

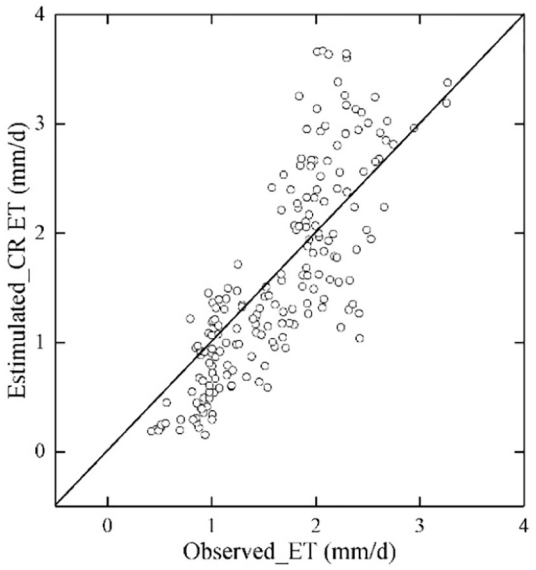

Fig. 4. Comparison of observed daily ET and simulated ET by CR model, at the Ordos Station.

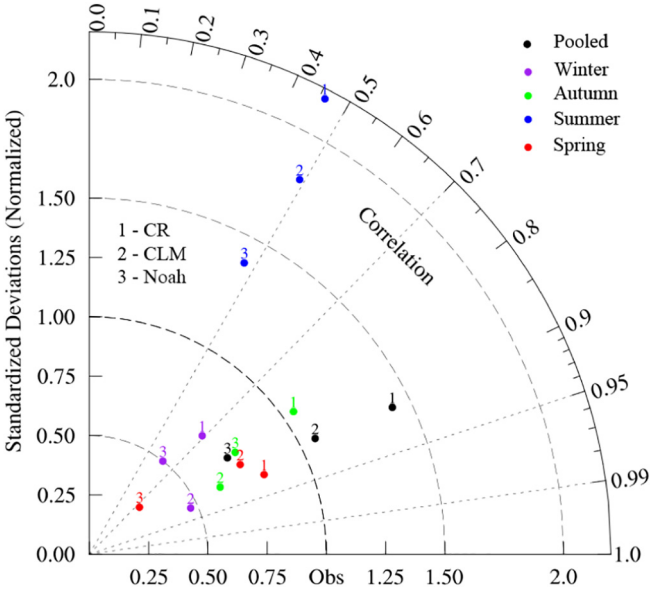

Fig. 6. The Taylor-diagram shows seasonal and pooled performance of three models driven by WRF, at the Yanchi Station. The Pearson correlation coefficient (r), root-mean-square deviation (RMSD), and standard deviation (SD) are calculated in the plots between simulated and observed datasets.

this area (Liu et al., 2010), the overall overestimation of air temperature leads to an underestimation of ET at the beginning of Fig. 4.

4.3. Comparison and verification of model simulations on ET

Fig. 5 shows the series of simulated daily ET values by the WRF-CLM4.0, WRF-Noah, the CR and the observed daily ET values for autumn (September–November) of 2016, winter (December 2016–February 2017), spring (March–May) of 2017 and summer (June–August) of 2017. In the Yanchi Observation Station, the three simulations show that the ET decreased from autumn to winter and increased from spring to summer. The simulation by the CR shows an underestimated ET values in autumn and the early spring in which the values of ET are relative low, but overestimated ET values in the late spring and summer, the period that values of ET begin to increase. In general, the CR simulation has a tendency to overestimate the ET when ET values are high and underestimate the ET when ET values are low and this phenomenon can also be seen in Fig. 4. The WRF-CLM4.0 model performed well in most of the days, with a few days of low bias in spring. It is worth noting that the CR model performed extraordinarily well compared to the other models in spring. The WRF-Noah model shows a low bias in most of the year. However, all three models performed relatively poor in summer.

The Taylor diagram (Taylor, 2001) is used to show the performance of ET simulated from WRF-CLM4.0, WRF-Noah and the CR as compared to the observed datasets (Fig. 6). The circle in the x axis, called reference point, represents the perfect fit between the modeled results and observations. The closer a label is to the reference point, the better the model performance.

The Taylor diagram shows the comparison of the simulated seasonal ET and observed ET. Overall, the WRF-CLM4.0 and CR simulated ET values showed a better performance compared to the WRF-Noah. In autumn, the CR and WRF-CLM4.0 show a better performance than the WRF-Noah in terms of correlation and standard deviation. In winter, the WRF-CLM4.0 shows a higher correlation than the WRF-Noah. This may be due to large snow pack in the study region (Jin and Wen, 2012). Meanwhile, WRF-Noah exhibits similar standard deviation which is close to one, indicating the same standard deviation value as that of the observations. In spring, the CR and WRF-CLM4.0 have comparable performances. The Noah simulations show a larger standard deviation with the furthest label to the reference point in Fig. 6.

In summer, all of the three models performed worse compared to the other seasons of the year. This may mainly attribute to the fact that the WRF model does not simulate the rain well in the summer (Lu and Kueppers, 2012; Jin et al., 2010). At the same time, the WRF-Noah simulation indicates a remarkable improvement in the standard deviation, with a standard deviation ratio of about one, indicating a relatively good agreement with the observations. Considering this

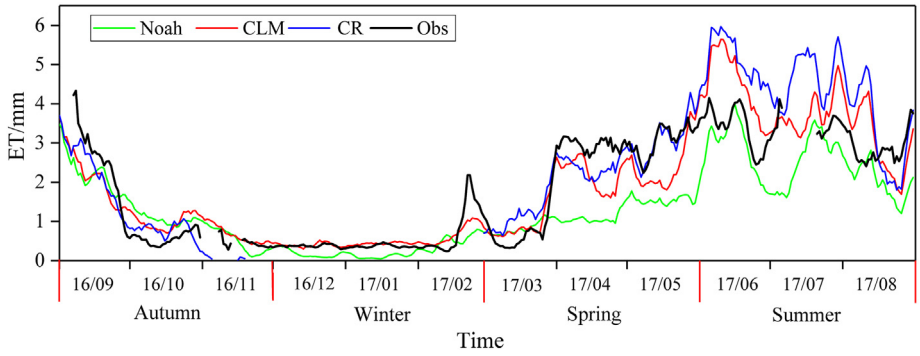

Fig. 5. Comparison of seasonal ET simulated by WRF-CLM4.0, WRF-Noah and CR models and observed actual ET at the Yanchi Station. The time series is from 1 September 2016 to 31 August 2017 including Autumn (September 2016 to November 2016), Winter (December 2016 to February 2017), Spring (March 2017 to May 2017) and Summer (June 2017 to August 2017).

situation, although the WRF-CLM4.0 and CR were more efficient in ET estimation, more researches are needed for applications of the WRF-Noah in the study region.

For quantitative evaluation, the consistency between seasonal and pooled simulations of the CR, WRF-CLM4.0 and WRF-Noah models with observed ET is given in Table 2. For seasonal behaviors, the WRF-CLM4.0 and WRF-Noah have better performances in autumn, while the CR shows the best behavior in spring. In winter, both the WRF-CLM4.0 and WRF-Noah show the best RMSE, but a very low correlation. The lower RMSE values in the two models were mainly attributable to the smaller magnitude of the ET ratio in winter among all the seasons. All the three models had their lowest agreement with the observations in the summer days with the lowest r values. Analyses of the pooled data also illustrated a better performance for the WRF-CLM4.0 (r = 0.89 [significant at $\alpha = 0.05$], RMSE = 0.66 mm/d, NSE = 0.90) and the CR simulations (r = 0.91 [significant at $\alpha = 0.05$], RMSE = 0.85 mm/d, NSE = 0.85) than the WRF-Noah performance (r = 0.82, [significant at $\alpha = 0.05$] RMSE = 0.94 mm/d, NSE = 0.81). The quantitative analysis of the pooled data demonstrated that the CR model and the WRF-CLM4.0 model outperformed the WRF-Noah simulations and show better applications on ET simulation in the study region.

4.4. Potential causes for different model performances

4.4.1. Model structure: hydrology

In semi-arid area, soil moisture is the dominant factor affecting ET (Xu and Singh, 2005). As can be seen from formulas (1)–(14), (16)–(22), soil moisture affects ET in the form of a power function in the CLM scheme, which is more sensitive than other factors, but in a linear form in the Noah scheme. The CR model represents the surface moisture condition by the difference between the saturated water pressure and the actual water pressure. Our research area is under a semi-arid climate, where the relationship between soil moisture and evaporation is strongest because ET in the arid and semi-arid regions is basically limited by the soil moisture (Lawrence and Slingo, 2005; Wu and Dickinson, 2004), and is suitable for the application of the CLM model (Xiao et al., 2017). With higher sensitivity to soil moisture, the WRF-CLM4.0 model more appropriately describes the surface energy partitioning processes in semi-arid regions, resulting in a better ET simulation in most of the seasonal ET simulations, and our result is similar to the results of Xiao et al. (2017) and Yang et al., 2016a.

In winter months, the entire downward solar radiation ($S_g\downarrow$) in Eq. (23) is used for calculating the heat flux for melting snow, while a fractional downward solar radiation ($S_0\downarrow$) is assigned to snow surface exposed to the air according to the area weight in the WRF-CLM4.0 model, as shown in Eq. (15), leading to a faster snow melting process (Jin and Wen, 2012). In Winter Day 75 to Spring Day 10, the WRF-Noah model dramatically underestimated the ET since there was not much snow retained, which is similar to the research of Jin and Wen (2012). Based on heuristic arguments, the CR model simplifies the physical processes of ET in the semi-arid and arid regions (Ozdogan et al., 2006).

Table 2
Performance statistics of the simulated ET from the three models and observed ET at the Yanchi station at seasonal and pooled time scale.

	CR		CLM		Noah	
	r	RMSE	r	RMSE	r	RMSE
Autumn	0.82	0.56	0.89	0.44	0.82	0.49
Winter	0.69	0.62	0.91	0.06	0.62	0.16
Spring	0.91	0.24	0.86	0.52	0.73	2.01
Summer	0.46	2.17	0.49	0.98	0.47	0.83
Pooled	0.90	0.85	0.89	0.66	0.82	0.94

4.4.2. Model structure: land surface representation

In terms of model structure, heterogeneous land surfaces have variable land cover types and vegetation amounts, which will lead to differences in land surface processes, such as surface roughness, canopy transmission of light and physiological responses to environmental controls, all influencing the ET.

Fig. 5 shows that the WRF-Noah model has an underestimation of ET during the growing season of plant, and an overestimation in autumn after harvest from Autumn Day 26 to Autumn Day 70. This is because the WRF-Noah model has an inaccurately homogeneous representation of plant type functions as it assumes one dominant plant functional type in each grid cell and ignores the others in the research grid (Chen and Dudhia, 2001), resulting in a bias in the ET pattern caused by plant physiological processes (Van Den Broeke et al., 2018), while the WRF-CLM4.0 model performed better because of a subgrid configuration and a combination of the PTFs in each grid cell.

Consideration of the effect of human activities in ET estimation, such as irrigation, is an important function of model structure (Falk et al., 2014). Unfortunately, both the Noah model and the CLM model coupled to WRF don't have irrigation scheme (Van Den Broeke et al., 2018). In Day 60 to 90 of spring, an irrigation period in our research area (Zhu et al., 2019), the two land surface models underestimated the value of ET obviously, while the CR model remarkably captured the changes in soil moisture as a result of irrigation, making a better performance than the WRF-CLM4.0 and WRF-Noah. For the CR model, as can been seen in formula (24) and (25), the decrease in U_2 (because of increased surface roughness) (Ozdogan and Salvucci, 2004) and in vapor pressure deficit caused by irrigation leads to decrease in ET_p. And the complementary relationship hypothesized by Bouchet (1963) leads to increases in actual ET. In the mixed land surface of farmland and grassland, irrigation would change regional surface moisture conditions (soil moisture and vapor pressure). Through catching the increases in e_a and reduction in ET_p which only requires measured weather data, the CR approach could directly relates the ET to the atmospheric boundary layer and remarkably captures the effects of irrigation to regional actual ET in the APENC. Use of meteorological data and the local parameter validation makes the CR model sensitive to fairly rapid changes to land surface and lower boundary layer feedback.

4.4.3. Evaluation of model applicability

The statistic analysis indicated the WRF-CLM4.0 model and the CR model outperformed the WRF-Noah model in estimating ET values in the study region. This result supports the conclusion of research of Ma and Szilagyi (2019) in the United States that the CR model is more applicable on regional scale compared to other regional models. And it shows that the CR model can benefit with climate model and be regarded as a benchmark and diagnostic tool for the models with high complexity such as LSMs (Ma and Szilagyi, 2019). Appropriate model hydrology and structure make the WRF-CLM4.0 capture the main characteristics of the dry climate and heterogeneous land use cover in the study region. Although there is a lack of more accurate simulation of winter ET values, the ability of precisely catching the effects of irrigation in grid cells with heterogeneous land use cover and achieving a comparable performance with the WRF-CLM gives the CR a special advantage to study the agriculture management since the irrigation module in the CLM4.5 can not represent the soil moisture condition well in the study area (Zhu et al., 2019). Thus, the CR approach could be used to research the human influence on ET and to complement other methods.

For regional applications, as an empirical model with local parameter validation, the CR model is able to capture the local characteristic affecting the regional ET such as climate, soil moisture and vegetation management processes. At the same time, with global adjustment (Jin et al., 2010), the CLM land surface scheme may not reflect regional characteristics, such as crop strains and vegetation biophysical variables (Lu and Kueppers, 2012), accurately in specific areas. These affect the calculation of the regional ET. The application of the local calibration in the CR

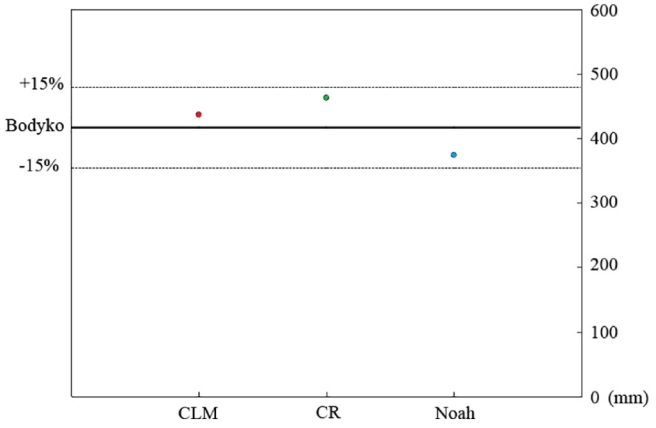

Fig. 7. The mean annul ET values of the study area simulated by the WRF-CLM4.0, CR, WRF-Noah models (the round dot) and the Budyko hydrological model (the bold line) from 2016 to 2017. The two dashed lines represent the ±15% relative errors.

model shows a good result in Fig. 3. It indicates that further promotion in regional applications of the CLM scheme may be achieved by local parameter validation.

4.4.4. Limitation of the study

Due to the lack of regional observations at daily intervals, this study was based only on data from two in situ observation stations for the period of 2016–2017. To overcome this limitation, we applied a Budyko model to estimate the mean annul ET value of the study area from a water balance approach. In the study area, the parameter α value of 2.3 was from a multi-year (50 years) water balance study by Gao et al. (2016). The mean annual ET derived by the Budyko model is 416 mm/year, which is consistent with previous researches in adjacent semi-arid area in the Loess Plateau (southeast of the study region) (Gao et al., 2016; Gao et al., 2017). As Fig. 7 shows, the simulated annual ET values by the three models (CLM, CR and Noah) are 437 mm, 463 mm and 374 mm, respectively, in agreement with the reference value of 416 mm/year by the Budyko model, with a relative error <15%. The above comparison indicates that our results are reasonable and consistent with other studies in the study region.

In the APENC region, the dominant land cover types are grassland and semi-arid farmland (Qi et al., 2012). Our study sites include Yachi Observation Station in the south and Ordos Observation Station within the National Field Station for Grassland Ecosystem in Ordos of China Ecological Research Network in the north, monitoring energy and water fluxes from both grassland and farmland. The two sites, while limited in numbers due to resource constraints, match the regional surface and environmental conditions of the APENC well and serve as microcosm of the APENC (Liu et al., 2019; Zhu et al., 2019). A multi-year (2014–2016) average ET value in growing season at Yulin Observation Station, which is also locate in the APENC, from Gong et al., 2018 is 327.7 mm, which is consistent with our 2016–2017 average ET value of 345.9 mm at the Yanchi Observation Station. Comparisons of the ET estimates by the WRF-CLM4.0, CR, and WRF-Noah models with the observed ET values in the Yanchi Observation Station show good agreement. Therefore, the results of this study, while still preliminary due to lack of the in situ observations, are representative of the study region, and once further verified, could be applied to the rest of the APENC.

5. Conclusion

Accurate estimation of the ET at regional scale is essential for effective management of the agricultural production and successful protection of grassland ecosystem in the highly heterogeneous and data lacking agricultural-pastoral ecotone in Northwest China. In this study, three models, the empirical CR model, intermediate WRF-Noah model and highly complex WRF-CLM4.0 model, were examined to estimate autumn (2016), winter (2016–2017), spring (2017), and summer (2017) ET values over daily intervals. The simulation results were evaluated and compared with the in situ observations. Results show that the WRF-CLM4.0 model exhibited the best performance, and the CR model has a comparable performance. The WRF-Noah model shows the worst performance. Thus, the highly complex WRF-CLM4.0 model and the empirical CR model seem to be better suited for estimating regional ET values in the APENC. For regional applications, the CR model, with fewer parameters and simpler structure, is able to capture the local characteristic affecting the regional ET such as climate, soil moisture and vegetation management processes, and is well-suited for data lacking, highly heterogeneous landscapes such as the APENC. Due to the lack of observations, this study was based only on data from two in situ observation stations for the period of 2016–2017. The results, while still preliminary, are consistent with studies in other dry areas. The initial findings, once verified in the field, could be applicable to other research areas with similar dry climate and heterogeneous land surface covers.

CRediT authorship contribution statement

Xuefeng Xu: Conceptualization, Methodology, Software, Writing - original draft.**Xuliang Li:**Data curation, Software.**Xuejin Wang:**Data curation, Software.**Chansheng He:**Project administration, Writing - review & editing.**Wei Tian:**Project administration.**Jie Tian:**Project administration.**Lixiao Yang:**Project administration.

Declaration of competing interest

No conflict of interest exits in the submission of this manuscript, and manuscript is approved by all authors for publication. I would like to declare on behalf of my co-authors that the work described was original research that has not been published previously, and not under consideration for publication elsewhere, in whole or in part. All the authors listed have approved the manuscript that is enclosed.

Acknowledgments

The project is partially funded by the National Natural Science Foundation of China (Grants: 41530752 and 91125010) and Scherer Endowment Fund of Department of Geography, Western Michigan University. We also acknowledge kind support by the National Field Station for Grassland Ecosystem in Ordos, Inner Mongolia, China. We thank the three anonymous reviewers for their constructive comments and suggestions.

References

Oleson, K.W., Lawrence, D.M., Gordon, B., Flanner, M.G., Kluzek, E., Peter, J., ... Heald, C.L., 2010. Technical description of version 4.0 of the Community Land Model (CLM). https://doi.org/10.2172/885637.

Allen, R.G., Pereira, L.S., Howell, T.A., Jensen, M.E., 2011. Evapotranspiration information reporting: I. Factors governing measurement accuracy. Agric. Water Manag. 98 (6), 899–920. https://doi.org/10.1016/j.agwat.2010.12.015.

Bouchet, R.J., 1963. Evapotranspiration réelle et potentielle, signification climatique. 62. IAHS Publ, pp. 134–142.. https://doi.org/10.1016/b978-0-08-009683-4.50069-3.

Branch, O., Warrach-Sagi, K., Wulfmeyer, V., Cohen, S., 2014. Simulation of semi-arid biomass plantations and irrigation using the WRF-NOAH model–a comparison with observations from Israel. Hydrol. Earth Syst. Sci. 18 (5), 1761–1783. https://doi.org/10.5194/hess-18-1761-2014.

Brustaert, W., 1982. Evaporation into the Atmosphere, Theory, History and Application. D. Reidel pub. Comp, Dordrecht-Boston-London https://doi.org/10.1007/978-94-017-1497-6_2.

Brutsaert, W., Stricker, H., 1979. An advection-aridity approach to estimate actual regional evapotranspiration. Water Resour. Res. 15 (2), 443–450. https://doi.org/10.1029/wr015i002p00443.

Budyko, M.I., 1974. Climate and Life. 508. Academic press, New York.

Cao, Q., Yu, D., Georgescu, M., Han, Z., Wu, J., 2015. Impacts of land use and land cover change on regional climate: a case study in the agro-pastoral transitional zone of China. Environ. Res. Lett. 10 (12), 124025. https://doi.org/10.1088/1748-9326/10/12/124025.

Chen, F., Dudhia, J., 2001. Coupling an advanced land surface–hydrology model with the Penn State–NCAR MM5 modeling system. Part I: model implementation and sensitivity. Mon. Weather Rev. 129 (4), 569–585. https://doi.org/10.1175/1520-0493(2001)129<0587:caalsh>2.0.co;2.

Chen, C., Huang, D., Wang, Q., Wu, J., Wang, K., 2016. Invasions by alien plant species of the agro-pastoral ecotone in northern China: species-specific and environmental determinants. J. Nat. Conserv. 34, 133–144. https://doi.org/10.1016/j.jnc.2016.10.004.

Clapp, R.B., Hornberger, G.M., 1978. Empirical equations for some soil hydraulic properties. Water Resour. Res. 14 (4), 601–604. https://doi.org/10.1029/wr014i004p00601.

Cruz-Blanco, M., Santos, C., Gavilán, P., Lorite, I.J., 2015. Uncertainty in estimating reference evapotranspiration using remotely sensed and forecasted weather data under the climatic conditions of southern Spain. Int. J. Climatol. 35 (11), 3371–3384. https://doi.org/10.1002/joc.4215.

Detto, M., Montaldo, N., Albertson, J.D., Mancini, M., Katul, G., 2006. Soil moisture and vegetation controls on evapotranspiration in a heterogeneous mediterranean ecosystem on Sardinia, Italy. Water Resour. Res. 42 (8), 1013–1016. https://doi.org/10.1029/2005wr004693.

Falk, M., Pyles, R.D., Ustin, S.L., Paw, U, T, K., Xu, L., Whiting, M.L., ... Brown, P.H., 2014. Evaluated crop evapotranspiration over a region of irrigated orchards with the improved ACASA–WRF model. Journal of Hydrometeorology 15 (2), 744–758. https://doi.org/10.1175/jhm-d-12-0183.1.

Fisher, J.B., Melton, F., Middleton, E., Hain, C., Anderson, M., Allen, R., Kilic, A., 2017. The future of evapotranspiration: global requirements for ecosystem functioning, carbon and climate feedbacks, agricultural management, and water resources. Water Resour. Res. 53 (4), 2618–2626. https://doi.org/10.1002/2016wr020175.

Fu, B.P., 1981. On the calculation of the evaporation from land surface. Sci. Atmos. Sin 5 (1), 23–31 (in Chinese).

Fu, B., Liu, Y., Lü, Y., He, C., Zeng, Y., Wu, B., 2011. Assessing the soil erosion control service of ecosystems change in the loess plateau of China. Ecol. Complex. 8 (4), 284–293. https://doi.org/10.1016/j.ecocom.2011.07.003.

Gao, G., Fu, B., Wang, S., Liang, W., Jiang, X., 2016. Determining the hydrological responses to climate variability and land use/cover change in the Loess Plateau with the Budyko framework. Sci. Total Environ. 557–558, 331–342. https://doi.org/10.1016/j.scitotenv.2016.03.019.

Gao, X., Sun, M., Zhao, Q., Wu, P., Zhao, X., Pan, W., Wang, Y., 2017. Actual ET modelling based on the Budyko framework and the sustainability of vegetation water use in the loess plateau. Sci. Total Environ. 579, 1550–1559. https://doi.org/10.1016/j.scitotenv.2016.11.163.

Gong, T., Lei, H., Yang, D., Jiao, Y., Yang, H., 2017. Monitoring the variations of evapotranspiration due to land use/cover change in a semiarid shrubland. Hydrol. Earth Syst. Sci. 21 (2), 863–877. https://doi.org/10.5194/hess-2016-490-ac1.

Gong, T., Lei, H., Yang, D., Yang, H., Liu, T., Duan, L., 2018. Assessing impacts of extreme water and temperature conditions on carbon fluxes in two desert shrublands. Journal of Hydroelectric Engineering 37 (2), 32–46 (in Chinese).

Huang, L., Xiao, T., Zhao, Z., Sun, C., Liu, J., Shao, Q., Wang, J., 2013. Effects of grassland restoration programs on ecosystems in arid and semiarid China. J. Environ. Manag. 117, 268–275. https://doi.org/10.1016/j.jenvman.2012.12.040.

Huntington, J.L., Szilagyi, J., Tyler, S.W., Pohll, G.M., 2011. Evaluating the complementary relationship for estimating evapotranspiration from arid shrublands. Water Resour. Res. 47 (5). https://doi.org/10.1029/2010wr009874.

IPCC, 2014. Climate change 2014: Impacts, adaptation, and vulnerability. Part A: Global and Sectoral Aspects, Contribution of Working GroupII to the Fifth Assessment Report of the Intergovernmental Panel on Climate Change. Cambridge Univ. Press, Cambridge, U. K 1132 pp.

Jacquemin, B., Noilhan, J., 1990. Sensitivity study and validation of a land surface parameterization using the HAPEX-MOBILHY data set. Bound.-Layer Meteorol. 52 (1–2), 93–134. https://doi.org/10.1007/bf00123180.

Jaksa, W.T., Sridhar, V., Huntington, J.L., Khanal, M., 2013. Evaluation of the complementary relationship using Noah Land Surface Model and North American Regional Reanalysis (NARR) data to estimate evapotranspiration in semiarid ecosystems. J. Hydrometeorol. 14 (1), 345–359. https://doi.org/10.1175/jhm-d-11-067.1.

Jin, J., Wen, L., 2012. Evaluation of snowmelt simulation in the weather research and forecasting model. Journal of Geophysical Research: Atmospheres 117. https://doi.org/10.1029/2011jd016980.

Jin, J., Miller, N.L., Schlegel, N., 2010. Sensitivity study of four land surface schemes in the WRF model. Adv. Meteorol. 2010. https://doi.org/10.1155/2010/167436.

Kahler, D.M., Brutsaert, W., 2006. Complementary relationship between daily evaporation in the environment and pan evaporation. Water Resour. Res. 42 (5). https://doi.org/10.1029/2005wr004541.

Kioutsioukis, I., de Meij, A., Jakobs, H., Katragkou, E., Vinuesa, J.F., Kazantzidis, A., 2016. High resolution WRF ensemble forecasting for irrigation: multi-variable evaluation. Atmos. Res. 167, 156–174. https://doi.org/10.1016/j.atmosres.2015.07.015.

Lawrence, D.M., Slingo, J.M., 2005. Weak land–atmosphere coupling strength in HadAM3: the role of soil moisture variability. J. Hydrometeorol. 6 (5), 670–680. https://doi.org/10.1175/jhm445.1.

Li, P., Li, B., 2000. Study on some characteristics of evaporation of sand dune and evapotranspiration of grassland in Mu Us desert. J. Hydraul. Eng. 3 (3), 24–28. https://doi.org/10.2480/agrmet.44.301.

Li, Xuliang, LiXiao, Yang, Wei, Tian, Xuefeng, Xu, He, chansheng, 2018a. Land use and land cover change in agro-pastoral ecotone in Northwest China: a review. Chin. J. Appl. Ecol. 29 (10), 3487–3495. https://doi.org/10.13287/j.1001-9332.201810.020 (in Chinese).

Li, S., Sun, Z., Tan, M., Guo, L., Zhang, X., 2018b. Changing patterns in farming–pastoral ecotones in China between 1990 and 2010. Ecol. Indic. 89, 110–117. https://doi.org/10.1016/j.ecolind.2018.01.067.

Liang, P., Yang, X., 2016. Landscape spatial patterns in the Maowusu (Mu Us) Sandy Land, northern China and their impact factors. Catena 145, 321–333. https://doi.org/10.1016/j.catena.2016.06.023.

Liang, X., Lettenmaier, D.P., Wood, E.F., Burges, S.J., 1994. A simple hydrologically based model of land surface water and energy fluxes for general circulation models. Journal of Geophysical Research Atmospheres 99 (D7), 14415–14428. https://doi.org/10.1029/94jd00483.

Liu, S., Bai, J., Jia, Z., Jia, L., Zhou, H., Lu, L., 2010. Estimation of evapotranspiration in the mu us Sandland of China. Hydrol. Earth Syst. Sci. 14 (3), 573–584. https://doi.org/10.5194/hess-14-573-2010.

Liu, P., Zha, T., Jia, X., Black, T.A., Jassal, R.S., Ma, J., Wu, Y., 2019. Different effects of spring and summer droughts on ecosystem carbon and water exchanges in a semiarid Shrubland ecosystem in Northwest China. Ecosystems 22 (8), 1869–1885. https://doi.org/10.1007/s10021-019-00379-5.

Lu, Y., Kueppers, L.M., 2012. Surface energy partitioning over four dominant vegetation types across the United States in a coupled regional climate model (weather research and forecasting model 3–community land model 3.5). Journal of Geophysical Research: Atmospheres 117 (D6). https://doi.org/10.1029/2011jd016991.

Ma, N., Szilagyi, J., 2019. The CR of evaporation: a calibration-free diagnostic and benchmarking tool for large-scale terrestrial evapotranspiration modeling. Water Resour. Res. https://doi.org/10.1029/2019wr024867.

Ma, Y., Zhu, Z., Zhong, L., Wang, B., Han, C., Wang, Z., Hu, Z., 2014. Combining MODIS, AVHRR and in situ data for evapotranspiration estimation over heterogeneous landscape of the Tibetan Plateau. Atmos. Chem. Phys. 14 (3), 1507–1515. https://doi.org/10.5194/acp-14-1507-2014.

Ma, N., Zhang, Y., Szilagyi, J., Guo, Y., Zhai, J., Gao, H., 2015. Evaluating the complementary relationship of evapotranspiration in the alpine steppe of the Tibetan Plateau. Water Resour. Res. 51 (2), 1069–1083. https://doi.org/10.1002/2014wr015493.

Monteith, J.L., 1963. Gas exchange in plant communities. Environmental Control of Plant Growth, pp. 95–112. https://doi.org/10.1016/b978-0-12-244350-3.50011-2.

Oleson, K., Dai, Y., Bonan, B., Bosilovichm, M., Dickinson, R., Dirmeyer, P., ... Thornton, P., 2004. Technical description of the community land model (CLM). University Corporation for Atmospheric Research https://doi.org/10.5065/D6N877R0 (No. NCAR/TN-461+STR).

Ozdogan, M., Salvucci, G.D., 2004. Irrigation-induced changes in potential evapotranspiration in southeastern Turkey: test and application of Bouchet's complementary hypothesis. Water Resour. Res. 40 (4). https://doi.org/10.1029/2003wr002822.

Ozdogan, M., Salvucci, G.D., Anderson, B.T., 2006. Examination of the Bouchet-Morton complementary relationship using a mesoscale climate model and observations under a progressive irrigation scenario. J. Hydrometeorol. 7 (2), 235–251. https://doi.org/10.1175/jhm485.1.

Pan, X., Li, X., Shi, X., Han, X., Luo, L., Wang, L., 2012. Dynamic downscaling of near-surface air temperature at the basin scale using WRF-a case study in the Heihe river basin, China. Frontiers of Earth Science 6 (3), 314–323. https://doi.org/10.1007/s11707-012-0306-2.

Penman, H.L., 1948. Natural evaporation from open water, bare soil and grass. Proceedings of the Royal Society of London. Series A. Mathematical and Physical Sciences 193 (1032), 120–145. https://doi.org/10.1098/rspa.1948.0037.

Perrin, C., Michel, C., Andréassian, V., 2001. Does a large number of parameters enhance model performance? Comparative assessment of common catchment model structures on 429 catchments. J. Hydrol. 242 (3–4), 275–301. https://doi.org/10.1016/s0022-1694(00)00393-0.

Philip, J.R., 1957. Evaporation, and moisture and heat fields in the soil. J. Meteorol. 14 (4), 354–366. https://doi.org/10.1175/1520-0469(1957)014<0354:eamahf>2.0.co;2.

Priestley, C.H.B., Taylor, R.J., 1972. On the assessment of surface heat flux and evaporation using large-scale parameters. Mon. Weather Rev. 100 (2), 81–92. https://doi.org/10.1175/1520-0493(1972)100<0081:otaosh>2.3.co;2.

Qi, Y., Chang, Q., Jia, K., Liu, M., Liu, J., Chen, T., 2012. Temporal-spatial variability of desertification in an agro-pastoral transitional zone of northern Shaanxi Province, China. Catena 88 (1), 37–45. https://doi.org/10.1016/j.catena.2011.08.003.

Reynolds, J.F., Smith, D.M.S., Lambin, E.F., et al., 2007. Global desertification: building a science for dryland development. Science 316 (2007), 847–851.

Sakaguchi, K., Zeng, X., 2009. Effects of soil wetness, plant litter, and under-canopy atmospheric stability on ground evaporation in the Community Land Model (CLM3. 5). Journal of Geophysical Research: Atmospheres 114 (D1). https://doi.org/10.1029/2008jd010834.

Simolo, C., Brunetti, M., Maugeri, M., Nanni, T., 2010. Improving estimation of missing values in daily precipitation series by a probability density function-preserving approach. Int. J. Climatol. 30 (10), 1564–1576. https://doi.org/10.1002/joc.1992.

Skamarock, W.C., Klemp, J.B., Dudhia, J., Gill, D.O., Barker, D.M., Wang, W., Powers, J.G., 2008. A Description of the Advanced Research WRF Version 3. NCAR Technical Note-475+ STR. http://citeseerx.ist.psu.edu/viewdoc/download?doi=10.1.1.484.3656&rep=rep1&type=pdf.

Smirnova, T.G., Brown, J.M., Benjamin, S.G., 1996. The soil component of the MAPS model: description and performance in one-and three-dimensional applications. Preprints, 11th Conf. On Numerical Weather Prediction. Amer. Meteor. Soc, Norfolk, VA, pp. 259–261.

Srivastava, P.K., Han, D., Islam, T., Petropoulos, G.P., Gupta, M., Dai, Q., 2016. Seasonal evaluation of evapotranspiration fluxes from MODIS satellite and mesoscale model downscaled global reanalysis datasets. Theor. Appl. Climatol. 124 (1–2), 461–473. https://doi.org/10.1007/s00704-015-1430-1.

Subin, Z.M., Riley, W.J., Jin, J., Christianson, D.S., Torn, M.S., Kueppers, L.M., 2011. Ecosystem feedbacks to climate change in California: development, testing, and analysis using a coupled regional atmosphere and land surface model (WRF3-CLM3.5). Earth Interact. 15 (15), 1–38. https://doi.org/10.1175/2010ei331.1.

Taylor, K.E., 2001. Summarizing multiple aspects of model performance in a single diagram. Journal of Geophysical Research: Atmospheres 106 (D7), 7183–7192. https://doi.org/10.1029/2000jd900719.

Thakur, J.K., Srivastava, P.K., Singh, S.K., Vekerdy, Z., 2012. Ecological monitoring of wetlands in semi-arid region of Konya closed Basin, Turkey. Reg. Environ. Chang. 12 (1), 133–144. https://doi.org/10.1007/s10113-012-0301-x.

Van Den Broeke, M.S., Kalin, A., Alavez, J.A.T., Oglesby, R., Hu, Q., 2018. A warm-season comparison of WRF coupled to the CLM4. 0, Noah-MP, and bucket hydrology land surface schemes over the central USA. Theor. Appl. Climatol. 134 (3–4), 801–816. https://doi.org/10.1007/s00704-017-2301-8.

Wang, K., Dickinson, R.E., 2012. A review of global terrestrial evapotranspiration: observation, modeling, climatology, and climatic variability. Rev. Geophys. 50 (2). https://doi.org/10.1029/2011rg000373.

Wang, X., Zhang, B., Xu, X., Tian, J., He, C., 2020. Regional water-energy cycle response to land use/cover change in the agro-pastoral ecotone, Northwest China. J. Hydrol., 124246 https://doi.org/10.1016/j.jhydrol.2019.124246.

Wei, B.C., Xie, Y.W., Jia, X., Wang, X.Y., He, H.J., Xue, X.Y., 2018. Land use/land cover change and it's impacts on diurnal temperature range over the agricultural pastoral ecotone of Northern China. Land Degrad. Dev. 29 (9), 3009–3020.

Wu, W., Dickinson, R.E., 2004. Time scales of layered soil moisture memory in the context of land-atmosphere interaction. J. Clim. 17 (14), 2752–2764. https://doi.org/10.1175/1520-0442(2004)017<2752:tsolsm>2.0.co;2.

Wu, F., Zhan, J., Yan, H., Shi, C., Huang, J., 2013. Land cover mapping based on multisource spatial data mining approach for climate simulation: a case study in the farming-pastoral ecotone of North China. Adv. Meteorol. 2013. https://doi.org/10.1155/2013/520803.

Wu, X., Shen, Y., Wang, N., Pan, X., Zhang, W., He, J., Wang, G., 2016. Coupling the WRF model with a temperature index model based on remote sensing for snowmelt simulations in a river basin in the Altay Mountains, north-West China. Hydrol. Process. 30 (21), 3967–3977. https://doi.org/10.1002/hyp.10924.

Wu, L., Zuo, H., Feng, J., 2018. Numerical simulation of the impacts of groundwater irrigation over the North China Plain on regional climate. Acta Meteorologica Sinica 76 (4), 635–648.

Xiao, Y., Zhuguo, M.A., Mingxing, L.I., 2017. Evaluation of the parameterization of soil moisture influence on evapotranspiration in land surface models. Chin. J. Atmos. Sci. https://doi.org/10.3878/j.issn.1006-9895.1606.15290 (in Chinese).

Xu, C.Y., Singh, V.P., 2005. Evaluation of three complementary relationship evapotranspiration models by water balance approach to estimate actual regional evapotranspiration in different climatic regions. J. Hydrol. 308 (1–4), 105–121. https://doi.org/10.1016/j.jhydrol.2004.10.024.

Xu, L., Pyles, R.D., Snyder, R., Monier, E., Falk, M., Chen, S.H., 2017. Impact of canopy representations on regional modeling of evapotranspiration using the WRF-ACASA coupled model. Agric. For. Meteorol. 247, 79–92. https://doi.org/10.1016/j.agrformet.2017.07.003.

Yang, Y., Qidong, Y., Xuying, S., Lijuan, W., 2016a. A comparative research of the simulation capability of noah, shaw, and clm models in semi-arid areas of northwestern China. Climatic & Environmental Research https://doi.org/10.3878/j.issn.1006-9585.2016.15105 (in Chinese).

Yang, Z., Zhang, Q., Yang, Y., Hao, X., Zhang, H., 2016b. Evaluation of evapotranspiration models over semi-arid and semi-humid areas of China. Hydrol. Process. https://doi.org/10.1002/hyp.10824 n/a-n/a.

Zhao, W., Hu, Z., Li, S., Guo, Q., Liu, Z., Zhang, L., 2017. Comparison of surface energy budgets and feedbacks to microclimate among different land use types in an agro-pastoral ecotone of northern China. Sci. Total Environ. 599, 891–898. https://doi.org/10.1016/j.scitotenv.2017.04.200.

Zhu, Yuzuo, Zhang, Lanhui, Tan, Xingyan, Zhu, Yi, Han, Zhibo, He, Chansheng, 2019. Evaluation of simulation performance of CLM4.5 at the Yanchi Station in the agricultural-pastoral Ecotone of Northwest China. Journal of Arid Meteorology https://doi.org/10.11755/j.issn.1006-7639(2019)-03-0430 (in Chinese).